CONFIDENTIAL

NACA

RESEARCH MEMORANDUM

for the

Bureau of Ordnance, Department of the Navy

FLIGHT INVESTIGATION TO EVALUATE THE ROLL-RATE STABILIZATION SYSTEM OF THE NAVAL ORDNANCE TEST STATION SIDEWINDER MISSILE AT MACH NUMBERS FROM 0.9 TO 2.3

By Clarence A. Brown, Jr., and Martin L. Nason

Langley Aeronautical Laboratory
Langley Field, Va.

NATIONAL ADVISORY COMMITTEE
FOR AERONAUTICS
WASHINGTON

CONFIDENTIAL

NACA RM SL54D26

NATIONAL ADVISORY COMMITTEE FOR AERONAUTICS

RESEARCH MEMORANDUM

for the

Bureau of Ordnance, Department of the Navy

FLIGHT INVESTIGATION TO EVALUATE THE ROLL-RATE STABILIZATION SYSTEM OF THE NAVAL ORDNANCE TEST STATION SIDEWINDER MISSILE AT MACH NUMBERS FROM 0.9 TO 2.3

By Clarence A. Brown, Jr., and Martin L. Nason

SUMMARY

A flight investigation using a rocket-powered model has been made to evaluate the roll-rate stabilization of the Naval Ordnance Test Station SIDEWINDER missile. This missile utilizes aerodynamic damping by gyro-actuated rollerons. Preliminary roll analysis indicated that a high-frequency dynamic roll instability would be produced by the rollerons.

This investigation indicated that a dynamic roll instability occurred in flight. The results also indicated that a dynamic roll-rate stabilization system roll-rate stabilized the missile within ±20 degrees per second through the proposed operating Mach number range of 0.9 to 2.3. The rollerons also prevented the roll angle oscillation of the model from exceeding ±5°, with an undesirable feature being the self-sustained roll velocity oscillation.

The preliminary analytical study indicated some system modifications which may eliminate the dynamic instability of the oscillatory roots. These are enumerated as follows:

(a) Increasing the control surface damping.

(b) Decreasing the angular momentum of the gyro wheel.

(c) Decreasing the control surface effectiveness or increasing the spring constant of the control surface.

Since modifications (b) and (c) would decrease the roll-rate stabilization effectiveness, these changes may not be acceptable; therefore, further research seems necessary to evaluate modifications (b) and (c).

INTRODUCTION

At the request of the Bureau of Ordnance, Department of the Navy, the Langley Pilotless Aircraft Research Division has initiated a program to investigate the stability of the Naval Ordnance Test Station SIDEWINDER missile. This missile utilized aerodynamic damping by gyro-actuated ailerons, hereafter called rollerons. Airstream-impelled gyro wheels, housed inside the roll control surfaces, comprise the complete roll stabilization system; therefore, no reference or rate-gyro roll control systems are required. These roll control surfaces are located at the trailing-edge tips of the trapezoidal wings of the model. Specifications for the design of the roll control system are given in reference 1.

Preliminary roll analysis of this missile indicated that a high-frequency dynamic roll instability would be produced by this type of roll-rate stabilization system. This paper presents the results of this roll analysis and the results of the flight test investigation to confirm the roll studies through a Mach number range of 0.9 to 2.3. Reference 1 gives the results of a preliminary evaluation of a roll-rate stabilization system similar to the one used in this test.

The model used in this investigation was similar to the Naval Ordnance Test Station missile described in reference 2. The differences between the present Naval Ordnance Test Station SIDEWINDER missile and the one used in this investigation is a 3-inch section added ahead of the canard control surfaces.

Flight test of this model was conducted at the Langley Pilotless Aircraft Research Station at Wallops Island, Va.

SYMBOLS

R	Reynolds number, $\frac{VX}{\nu}$
X	length of model, ft
ν	kinematic viscosity, sq ft/sec
t	time, sec
M	Mach number
V	velocity of model, ft/sec
q	dynamic pressure, lb/sq ft

φ	model roll angle, deg
$\dot{\varphi}$	rolling velocity of model, deg/sec
$\dot{\varphi}_m$	mean value of roll velocity envelope of model, deg/sec
$\omega_{\dot{\varphi}}$	roll velocity frequency, cps
C_D	drag coefficient, $\frac{\text{Drag}}{qS_b}$
S_b	cross-sectional area of fuselage, sq ft
l	distance from model center line to rolleron center of gravity, ft
d	distance from rolleron center of gravity to rolleron hinge line, ft
δ_R	rolleron angular deflection, radians
L	rolling moment, ft-lb
H	rolleron hinge moment, ft-lb
ω_G	gyro-wheel angular velocity, radians/sec
L_D	load disturbance in roll, ft-lb
m_R	mass of rolleron, slugs
I_G	moment of inertia of gyro wheel about spin axis, slug-ft^2
I_R	moment of inertia of rolleron about hinge line, slug-ft^2
I_X	moment of inertia of missile about roll axis, slug-ft^2
H_{δ_R}	rolleron-hinge-moment parameter, $\frac{\partial H}{\partial \delta_R}$, ft-lb/radian
L_{δ_R}	rolleron control effectiveness parameter, $\frac{\partial L}{\partial \delta_R}$, ft-lb/radian

$L_{\dot{\phi}}$ missile roll damping, $\frac{\partial L}{\partial \dot{\phi}}$, ft-lb/radian/sec

$H_{\dot{\delta}_R}$ rolleron control surface damping, $\frac{\partial H}{\partial \dot{\delta}_R}$, ft-lb/radian/sec

$D = \frac{d}{dt}$

A dot over a symbol denotes a derivative with respect to time.

APPARATUS AND METHODS

Model Description

Sketches of the rocket-powered model used in this test are shown in figure 1. Sketches of the canard surface and wing surface with attached rolleron are shown in figure 2. Photographs of the model and rollerons are shown in figures 3, 4, and 5.

The body of the model had a maximum diameter of 5 inches with a fineness ratio of 21.33. The fuselage was cylindrical with a spherical nose section. The nose section consisted of a 2.6-inch-radius spherical segment that was faired into the 5-inch-diameter body. The canard surfaces were located on the cylindrical portion of the model. (See figs. 1 and 3.) The canard surfaces were of 66° 37' delta-wing plan form with a modified single-wedge airfoil section having a constant thickness of 0.125 inch (fig. 2). The canard surfaces were welded to the steel skin and fixed at a zero angle of incidence. The wings were of trapezoidal plan form with the leading edge swept back 45° (fig. 2). The wing had a modified hexagonal airfoil section with a constant thickness corresponding to a thickness ratio of 1.2 percent at the wing-body juncture. The roll-rate stabilization controls, that is, the rollerons, were located at the trailing-edge tips of the model wings (figs. 2 and 4). The rollerons were rectangular in shape and each rolleron casing was designed to accommodate a gyro wheel 3 inches in diameter (fig. 2). The gyro wheels were constructed of steel and the periphery of each gyro wheel was notched with a series of 24 buckets. The rollerons were designed to be free to move about the rolleron hinge line with negligible friction.

Preflight Measurements and Checks

The values determined by preflight measurements are as follows:

Weight, lb (model sustainer loaded)	148.5
Weight, lb (model sustainer empty)	105.0
Moment of inertia:	
Model, sustainer empty, I_Y, slug-ft^2	31.08
Model, sustainer empty, I_X, slug-ft^2	0.30
Center-of-gravity location, model sustainer empty, in. from nose	49.75
Center-of-gravity location, model sustainer loaded, in. from nose	55.63

Prior to the flight test of the model, the gyro wheels of the rollerons were given an initial rotational speed. Although the rotational speed of the gyro wheels corresponding to a typical operational launching condition of this missile is unknown, the initial speed given the gyro wheels is probably closer to the actual launching rotational speed of the gyro wheel than if no initial rotational speed had been applied. The initial rotational speed of the rollerons was accomplished by applying a source of air to each of the rollerons while the model was on the launcher and allowing this air supply to turn the rollerons until the model had moved clear of the launcher. Figure 5 shows the model and booster on the launcher and the arrangement used to apply the air to the rollerons prior to launching.

Instrumentation

The model was equipped with an NACA four-channel telemeter which transmitted a continuous record of the normal and transverse accelerations, and rate of yaw, and rate of roll obtained from rate gyros.

Model velocity was obtained from the CW Doppler radar and the model trajectory was determined through use of a modified SCR-584 radar tracking unit. A radiosonde released at the time of flight was used to obtain atmospheric data throughout the altitude range transversed by the model.

ACCURACY

The accuracy of the results considering possible cumulative errors in radar and telemeter data is believed to be within the limits listed below:

C_D	±0.05

The measured response of the two rate gyros used to measure rate of roll and rate of yaw are as follows:

	Undamped natural frequency, cps	Percent critical damping
Rate of yaw	50	70 ± 5
Rate of roll	50	70 ± 5

Although a dynamic error may exist in these instruments, the frequency of the oscillation and the mean amplitude are essentially unaffected.

METHOD OF ANALYSIS

An analysis method was adopted which indicated stability by utilizing charts relating the stability boundary to the aerodynamic hinge-moment parameter H_{δ_R} and the rolling effectiveness parameter L_{δ_R}. These charts have been drawn for three values of rolleron control surface damping $\left(H_{\dot{\delta}_R} = -0.10, -0.50, \text{ and } -1.0 \text{ ft-lb/radian/sec}\right)$ and for the expected operating range of the missile roll damping $\left(L_{\dot{\varphi}} = -0.05 \text{ and } -5.0 \text{ ft-lb/radian/sec}\right)$ and gyro-wheel spin rates of 10,000, 60,000 and 100,000 rpm. The equations of motion on which the stability-boundary plots are based are given as follows:

Hinge moment:

$$H_{\delta_R}\delta_R + H_{\dot{\delta}_R}\dot{\delta}_R + m_R l_d \frac{\ddot{\varphi}}{57.3} - I_G\omega_G \frac{\dot{\varphi}}{57.3} = I_R\ddot{\delta}_R \qquad (1)$$

Rolling moment:

$$L_D + L_{\dot{\varphi}} \frac{\dot{\varphi}}{57.3} + 4L_{\delta_R}\delta_R + 4m_R l_d \ddot{\delta}_R + 4I_G\omega_G\dot{\delta}_R = I_X \frac{\ddot{\varphi}}{57.3} \qquad (2)$$

This analysis is subject to the following limitations:

(a) The aerodynamic forces and moments are assumed to depend linearly on their respective variables and are assumed to be independent of the frequency of oscillation.

(b) The angular momentum vector of the gyro wheel is essentially perpendicular to the plane of the wing, $\cos \delta_R \approx 1.0$.

(c) No pitching or yawing motion of the missile is present.

(d) No longitudinal, lateral, or normal acceleration of the missile are present.

The formulation of the stability conditions from the equations of motion is given in appendix A. Charts of this type may be utilized to examine the effect of various system parameters on the static and dynamic characteristics of the overall system and may also be used as a basis for system improvements. Although this analysis is oversimplified, trends obtained on the basis of the above assumptions should be valid.

TEST

The primary purpose of the flight test conducted on this missile was to determine the stability of the roll stabilization system in operational use. Since the stability of the system was shown to be marginal by the preflight analysis, no provision was made to introduce a rolling-moment disturbance. The effectiveness of the system for overcoming induced rolling moments was therefore not obtained.

Performance specifications (ref. 1 and unpublished data) relative to the stability of the roll system are:

(1) Steady-state damped roll rate must be less than 1 radian/sec for a rocket subject to the following design limits:

(a) Altitude, sea level to 40,000 feet

(b) Mach number, 1.2 to 2.5

(2) Mean lifetime of transient-roll period must be less than 0.2 second.

The model was boosted to supersonic velocities by a solid-propellant rocket motor which delivered approximately 6,000 pounds of thrust for 3.0 seconds. A sustainer motor, made as an integral part of the model,

delivered approximately 3,000 pounds of thrust for 2.6 seconds and propelled the model to the peak Mach number of 2.3. The model was launched from the ground at an angle of approximately 60° to the horizontal.

RESULTS AND DISCUSSION

Data on the roll stability were obtained for the model tested for a Mach number range of 0.9 to 2.3. The Reynolds number of the test ranged from 20×10^6 to 114×10^6 based on the length of the body. Variation of the Reynolds number with Mach number for this test is shown in figure 6. Plots of the time histories of the model flight are presented in figures 7 and 8 as the variation of the velocity, Mach number, altitude, and dynamic pressure with time.

Presented in figure 9 are three typical portions of the telemeter record received from this flight. As may be seen in figure 9(a), a roll instability occurred at a Mach number of 2.05. Subsequent to the divergent roll velocity oscillation encountered at a Mach number of 2.05, the model exhibited a self-sustained oscillation in the roll velocity characterized by two predominant frequencies. (See fig. 9.) This self-sustained oscillation in the roll velocity was present throughout the remainder of the flight. The variation with time of the lower frequency of the rolling velocity $\omega_{\dot{\phi}}$, the half-amplitude of the roll-velocity envelope, and the mean value of the roll-velocity envelope $\dot{\phi}_m$ are presented in figures 10, 11, and 12, respectively. As may be seen in figure 10, the frequency of the roll velocity $\omega_{\dot{\phi}}$ increased rapidly during the divergent roll instability to 37 cycles per second at a Mach number of 1.90 ($t = 8.4$ sec) but as the model velocity decreased to a Mach number of 0.74 ($t = 8.4$ sec) the frequency decreased to 10 cycles per second. The half-amplitude of the roll-velocity envelope (fig. 11) increased during the roll instability to 500 degrees per second at a Mach number of 1.90 ($t = 19.7$ sec) but as the oscillation became self-sutained the half-amplitude of the roll-velocity envelope decreased rapidly to 200 degrees per second, oscillated between 200 and 300 degrees per second, then decreased to 200 degrees per second at a Mach number of 0.74 ($t = 19.7$ sec). Although the frequency and amplitude of the self-sustained oscillation were large (fig. 12), the mean amplitude of the roll velocity $\dot{\phi}_m$ was less than ±20 degrees per second from model-booster separation, $t = 3.3$ seconds, until the model coasted to a Mach number of 0.86. Below a Mach number of 0.86, the mean amplitude of the roll velocity increased to a value of approximately 200 degrees per second. This increase in the mean amplitude of the roll velocity below this Mach number cannot be explained. Another mode of motion not considered in the analysis, a possible reduction in the missile roll damping contributed

by the rollerons, aerodynamic nonlinearities, or other effects may have produced this increase in mean amplitude of the roll velocity. It may be seen from figures 10, 11, and 12 that although the model experienced a divergent roll oscillation produced by the rollerons and then a self-sustained oscillation throughout the remainder of the flight the roll rate was stabilized for these test conditions within ±20 degrees per second through a Mach number range of 0.9 to 2.3.

Integration of the roll-rate oscillation was performed to determine the roll amplitude experienced by the model. This roll angle oscillation of the model varied from approximately ±2.5° at a Mach number of 1.6 to ±5.0° at a Mach number of 0.6. From the above-mentioned results, it appears that a roll-rate stabilization system utilizing aerodynamic damping by gyro-actuated rollerons will give roll velocity stabilization and small roll angle oscillation with an undesirable feature being the divergent, then self-sustained, high-frequency roll-rate oscillation.

Figure 13 presents the variation of the drag coefficient, based on the fuselage cross-sectional area, obtained by differentiation of the velocity obtained from the CW Doppler radar and an estimated zero-lift drag coefficient with Mach number. As may be noted in figure 13 the general shape of the measured model drag is similar to the estimated zero-lift drag coefficient and is approximately 8 to 10 percent higher than the estimated zero-lift drag coefficient.

As mentioned previously in the "Method of Analysis" section, design charts were constructed to determine the static and dynamic stability of the rolleron system. These charts are shown in figures 14 to 19. The diagrams were plotted for three gyro-wheel spin rates: 10,000 rpm, 60,000 rpm, and 100,000 rpm. For each spin rate the minimum and maximum values of roll damping, -0.05 and -5.0 ft-lb/radian/sec, respectively, were used to compute the stability boundaries. In each chart the static and oscillatory boundaries are shown for three values of control surface damping: -0.10, -0.50, and -1.0 ft-lb/radian/sec.

The darkened region in each figure represents the estimated operating region determined from reference 4. A slight increase in the area defined by this reference was arbitrarily made to account for factors not considered by these analysis. The static characteristics are unaffected by changes to the control surface damping; however, modifications to the control surface damping do affect the dynamic response. (See fig. 14.) Examination of figures 14, 16, and 18 indicates for a control surface damping $H_{\dot{\delta}_R}$ of -0.10 ft-lb/radian/sec and a missile roll damping $L_{\dot{\phi}}$ of -0.05 ft-lb/radian/sec that as the gyro-wheel angular velocity ω_G, or angular momentum $\left(I_G = \text{Constant}\right)$, is increased the unstable oscillatory stability region is moved so that the estimated operating region is on the unstable side of the oscillatory boundary. Note also the beneficial

effects of the addition of control surface damping (see fig. 16) and the slight effect of inherent missile roll damping on the oscillatory stability boundaries. (Compare figs. 16 and 17.) A decrease in the control surface effectiveness L_{δ_R} or increasing the spring constant H_{δ_R} of the control surface will rotate the estimated operating region in a counterclockwise direction, figure 16, thus moving the operating region toward the stable side of the oscillatory boundary. Since the divergent roll oscillation detected on the flight test model exhibited the characteristics which would be obtained by operation on the unstable side of an oscillatory stability boundary, the use of these design charts as a guide to system improvement is probably valid. However, the exact position in these charts of the flight test model cannot be located since the gyro-wheel spin rate was not measured in flight. Nevertheless, the presence of an oscillatory instability is likely because the estimated operating region fell within the unstable region (figs. 16 to 19).

Elimination of the dynamic instability of the oscillatory roots may be obtained by making one or more of the following system modifications:

(a) Increasing the control surface damping $H_{\dot{\delta}_R}$

(b) Decreasing the angular momentum of the gyro wheel

(c) Decreasing the control surface effectiveness L_{δ_R} or increasing the spring constant H_{δ_R} of the control surface

Since modifications (b) and (c) would decrease the roll-rate stabilization effectiveness, these changes might not be acceptable; therefore, further research seems necessary to evaluate modifications (b) and (c).

CONCLUSIONS

Data obtained from the flight investigation of a rocket-powered model to evaluate the roll-rate stability of the Naval Ordnance Test Station SIDEWINDER missile utilizing aerodynamic damping by gyro-actuated rollerons indicate the following:

1. A dynamic roll instability was produced by the rollerons at a high supersonic speed and continued as a self-sustained roll velocity oscillation for the remainder of the flight.

2. The rollerons roll rate stabilized the model within ±20 degrees per second through the proposed operating Mach number range of 0.9 to 2.3.

3. The roll-angle oscillation of the model was less than ±5° through the proposed operating Mach number range of 0.9 to 2.3.

The flight test investigation substantiated a preliminary roll analysis of the rolleron system which indicated that a dynamic instability of the oscillatory roots was present. This analytical study also indicated system modifications which might eliminate this instability. These are enumerated as follows:

(a) Increasing the control surface damping

(b) Decreasing the angular momentum of the gyro wheel

(c) Decreasing the control surface effectiveness or increasing the spring constant of the control surface.

Since modifications (b) and (c) would decrease the roll-rate stabilization effectiveness, these changes may not be acceptable; therefore, further research seems necessary to evaluate modifications (b) and (c).

Langley Aeronautical Laboratory,
National Advisory Committee for Aeronautics,
Langley Field, Va., April 13, 1954.

Clarence A. Brown Jr.

Clarence A. Brown, Jr.
Aeronautical Research Scientist

Martin L. Nason
Aeronautical Research Scientist

Approved: Joseph A. Shortal
Joseph A. Shortal
Chief of Pilotless Aircraft Research Division

lso

[redacted]

APPENDIX A

An indication of the stability of the rolleron system may be ascertained by neglecting the pitching and yawing motion of the missile and considering only the rolling motion. A sketch of the rolleron system showing the two degrees of freedom $\left(\varphi \text{ and } \delta_R\right)$ and the sign convention adopted is given on figure 20. The equations of motion are as follows:

Hinge Moment:

$$H_{\delta_R}\delta_R + H_{\dot{\delta}_R}\dot{\delta}_R + m_R l_d \frac{\ddot{\varphi}}{57.3} - I_G\omega_G \frac{\dot{\varphi}}{57.3} = I_R\ddot{\delta}_R \tag{A1}$$

Rolling Moment:

$$L_D + L_{\dot{\varphi}} \frac{\dot{\varphi}}{57.3} + 4L_{\delta_R}\delta_R + 4m_R l_d\ddot{\delta}_R + 4I_G\omega_G\dot{\delta}_R = I_X \frac{\ddot{\varphi}}{57.3} \tag{A2}$$

Rewriting these equations using operator notation gives

$$\left(m_R l_d D^2 - I_G\omega_G D\right) \frac{\varphi}{57.3} + \left(-I_R D^2 + H_{\delta_R} D + H_{\delta_R}\right)\delta_R = 0$$

$$\left(I_X D^2 - L_{\dot{\varphi}} D\right) \frac{\varphi}{57.3} + \left(-4m_R l_d D^2 - 4I_G\omega_G D - 4L_{\delta_R}\right)\delta_R = L_D$$

Assuming that $4m_R l_d\ddot{\delta}_R \approx 0$, then the characteristic equation becomes

$$a_0 D^3 + a_1 D^2 + a_2 D + a_3 = 0$$

where

$a_0 = I_R I_X$

$a_1 = -I_R L_{\dot{\varphi}} - 4m_R l_d \left(I_G\omega_G\right) - I_X H_{\dot{\delta}_R}$

$a_2 = 4\left(I_G\omega_G\right)^2 - 4m_R l_d L_{\delta_R} + L_{\dot{\varphi}} H_{\dot{\delta}_R} - I_X H_{\delta_R}$

$a_3 = L_{\dot{\varphi}} H_{\delta_R} + 4L_{\delta_R}\left(I_G\omega_G\right)$

A stable system will result if, and only if, the following relationships between the coefficients of the above polynomial are satisfied at all times: (See ref. 3 for a formal derivation of these conditions.)

$$a_0 > 0$$

$$a_1 > 0$$

$$a_1 a_2 - a_0 a_3 > 0 \qquad \text{(oscillatory stability boundary)}$$

$$a_3 > 0 \qquad \text{(static stability boundary)}$$

The stability boundary plots shown in figures 14 to 19 are based on the above relationships and were calculated using the measured and invarient mass characteristics tabulated below:

$$m_R = 0.031 \text{ slugs}$$

$$d = 0.1289 \text{ ft}$$

$$l = 0.775 \text{ ft}$$

$$I_R = 0.0007046 \text{ slug-ft}^2$$

$$I_G = 0.000198 \text{ slug-ft}^2$$

$$I_X = 0.30 \text{ slug-ft}^2$$

Since no reliable data exist, at the present time, for the aerodynamic characteristics $\left(L_{\delta_R}, L_{\dot{\phi}}, H_{\delta_R}, \text{ and } H_{\dot{\delta}_R}\right)$, the stability-boundary plots were calculated using these parameters as the principal variables. Each figure has been plotted with H_{δ_R} as the ordinate and L_{δ_R} as the abscissa for three values of control surface damping $H_{\dot{\delta}_R}$. The effect of the inherent missile roll damping $L_{\dot{\phi}}$ and the gyro-wheel spin rate ω_G was determined by replotting each figure using the expected operating range of these two variables. The probable range of H_{δ_R} and L_{δ_R} expected in flight is represented by the darkened area in each figure.

REFERENCES

1. LaBerge, Walter B., and Drinkwater, W. Dale: Preliminary Evaluation of a Simplified Roll-Rate Stabilization System. NAVORD Rep. 1269 (NOTS 339), U. S. Naval Ord. Test Station (Inyokern, Calif.), Jan. 8, 1951.

2. Gregory, J. F.: Flight Test of SIDEWINDER Missiles EX-1-2 Serial No. 3 and Serial No. 4. Test Rep. 30-160 (NOTS No. 633), U. S. Naval Ord. Test Station (Inyokern, Calif.), Mar. 31, 1953.

3. Routh, Edward John: Dynamics of a System of Rigid Bodies. Part II. Sixth ed., rev. and enl., Macmillan and Co., Ltd., 1905, pp. 223-230.

4. Tucker, Warren A., and Nelson, Robert L.: Theoretical Characteristics in Supersonic Flow of Constant-Chord Partial-Span Control Surfaces on Rectangular Wings Having Finite Thickness. NACA TN 1708, 1948.

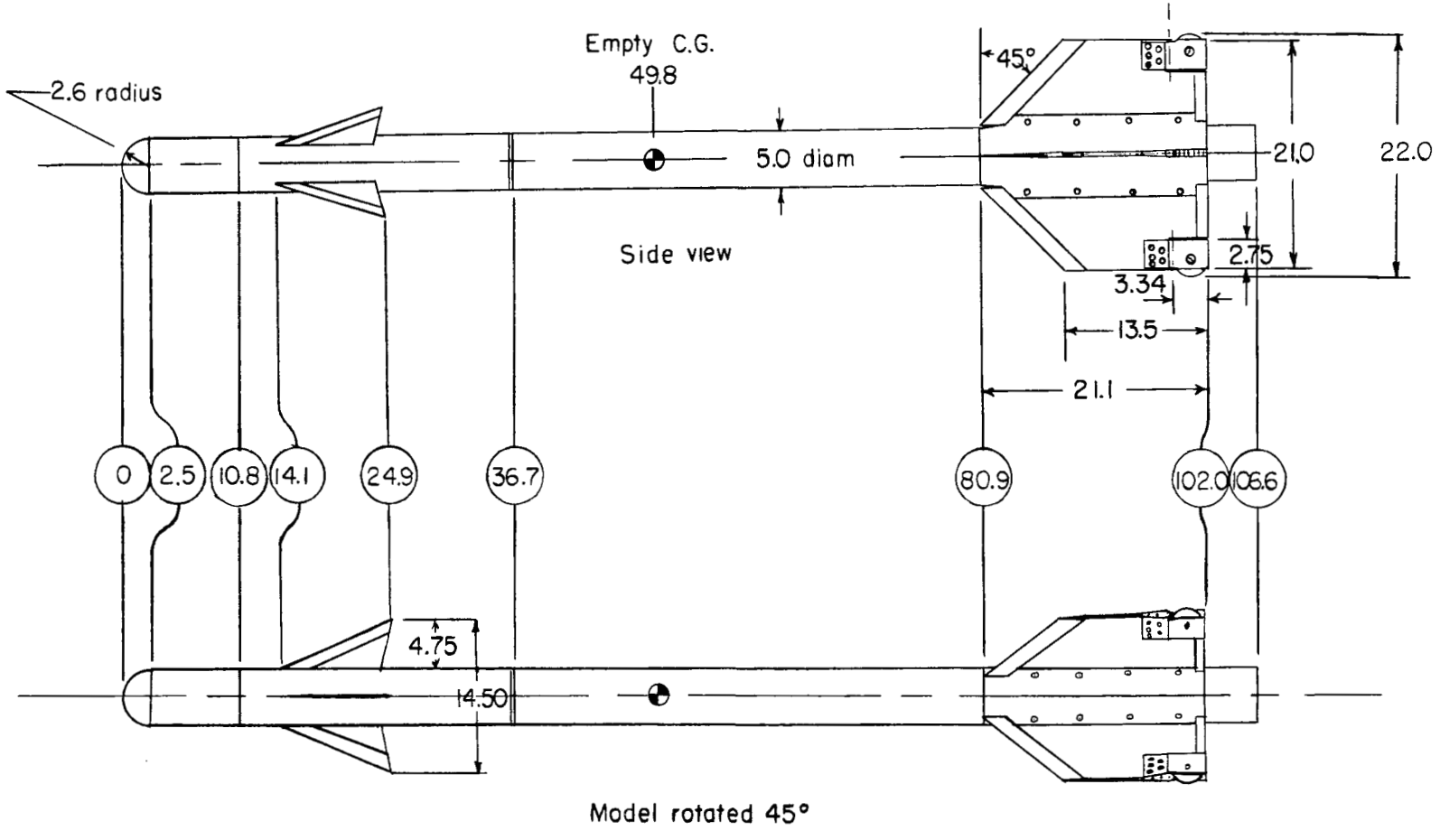

Figure 1.- Sketches of model tested with SIDEWINDER rollerons. All dimensions in inches.

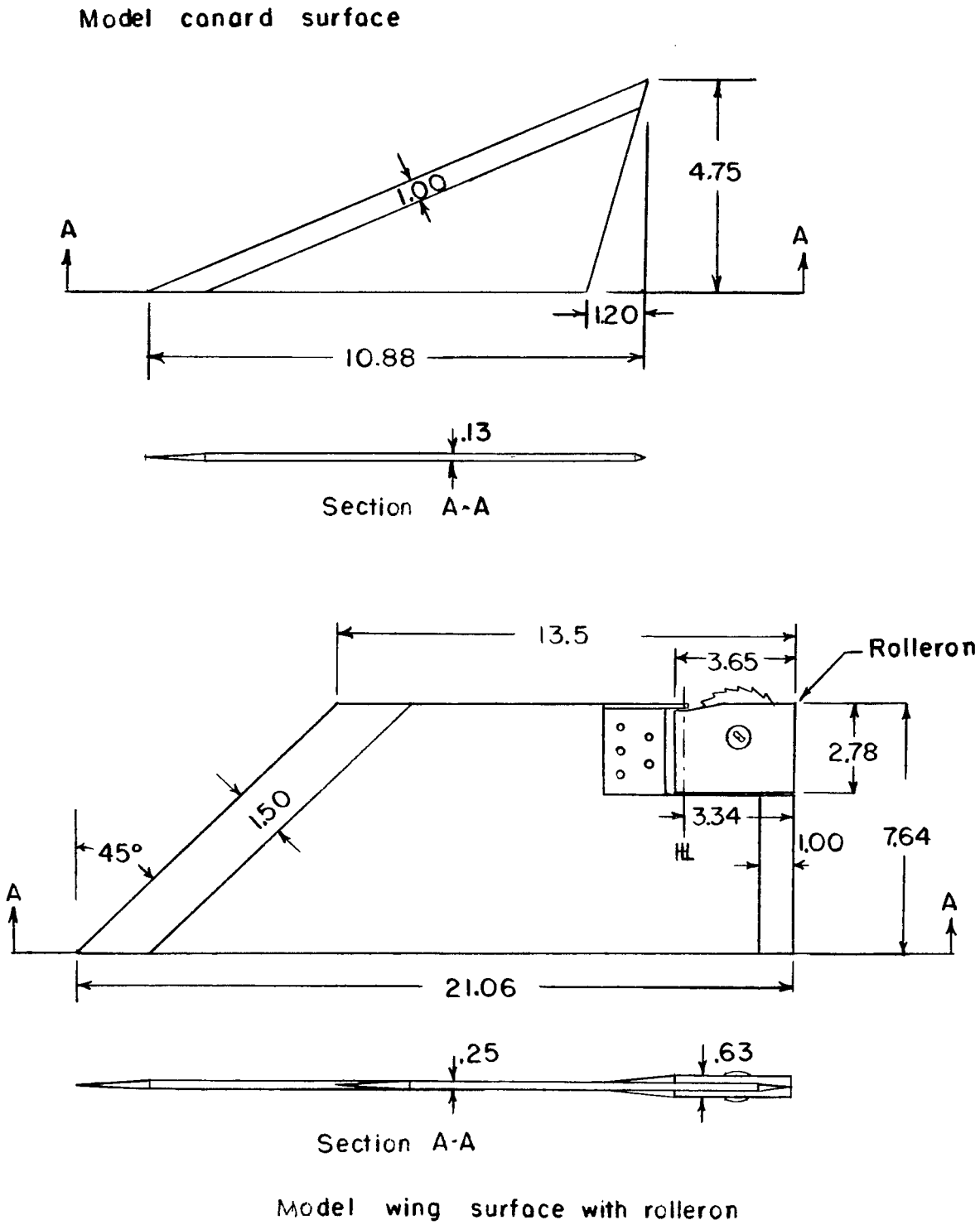

Figure 2.- Sketches of canard and wing with rolleron. All dimensions in inches.

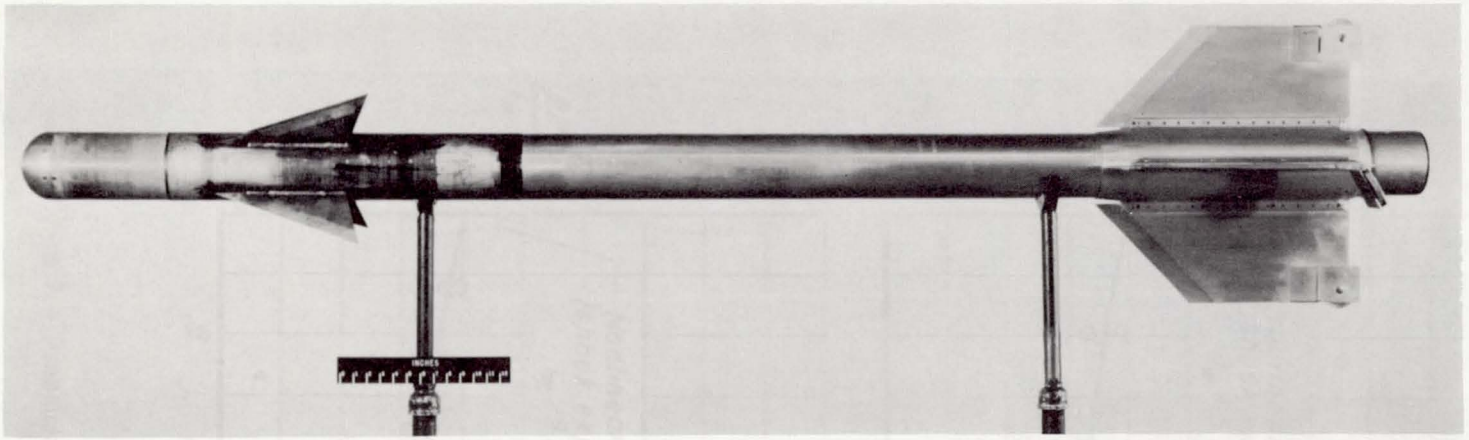

Side view

L-81853.1

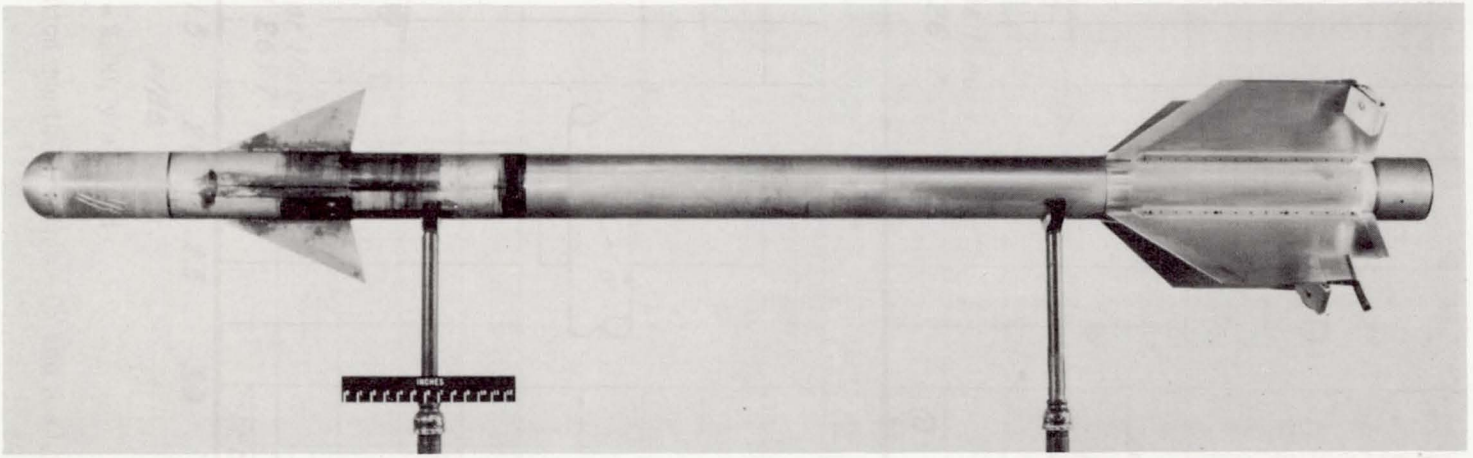

Model rotated 45°

L-81852.1

Figure 3.- Photographs of model tested with SIDEWINDER rollerons.

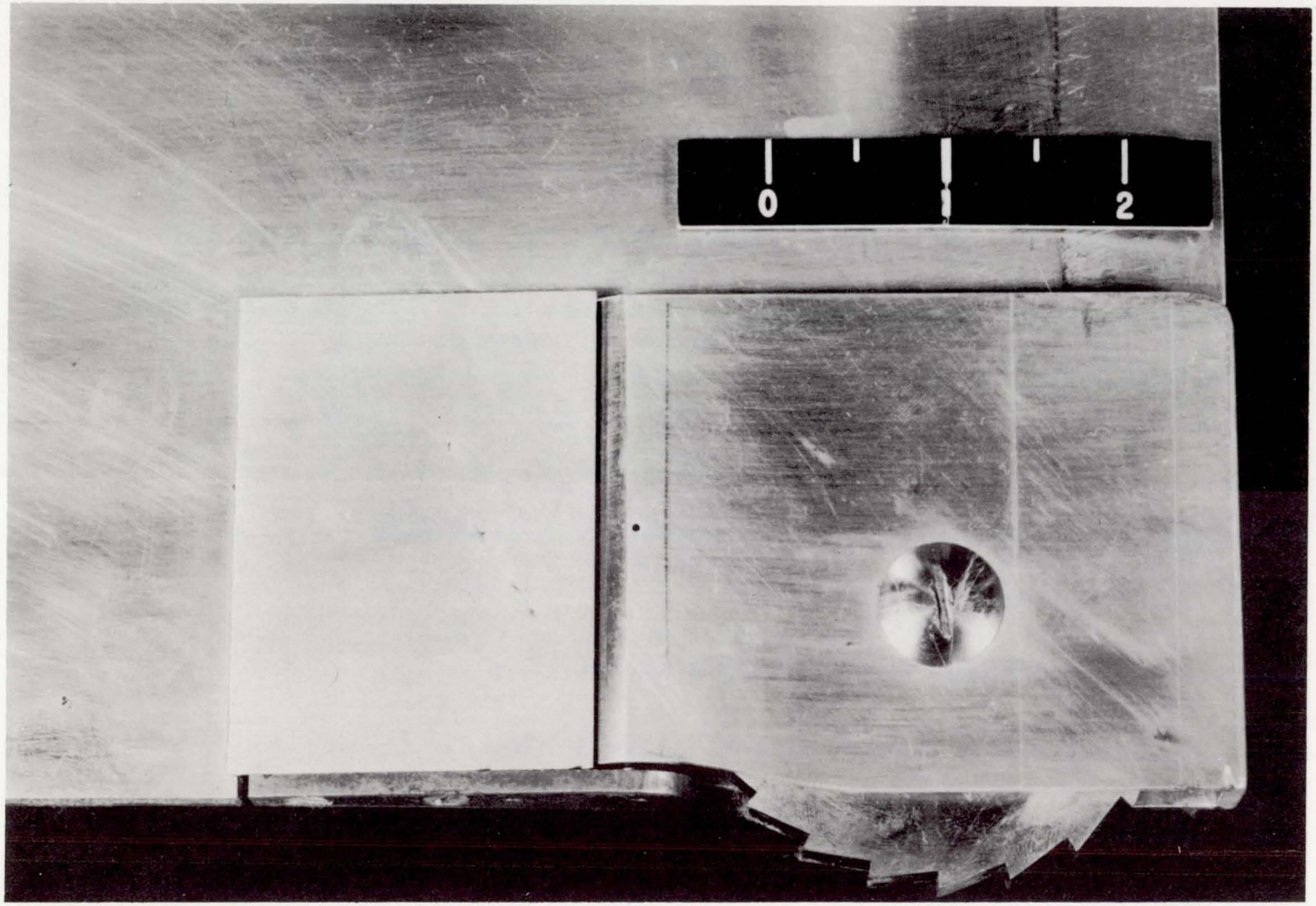

Figure 4.- Photograph of rollerons used on model tested. L-81854

L-82276.1

Figure 5.- Photograph of model and booster prior to launching.

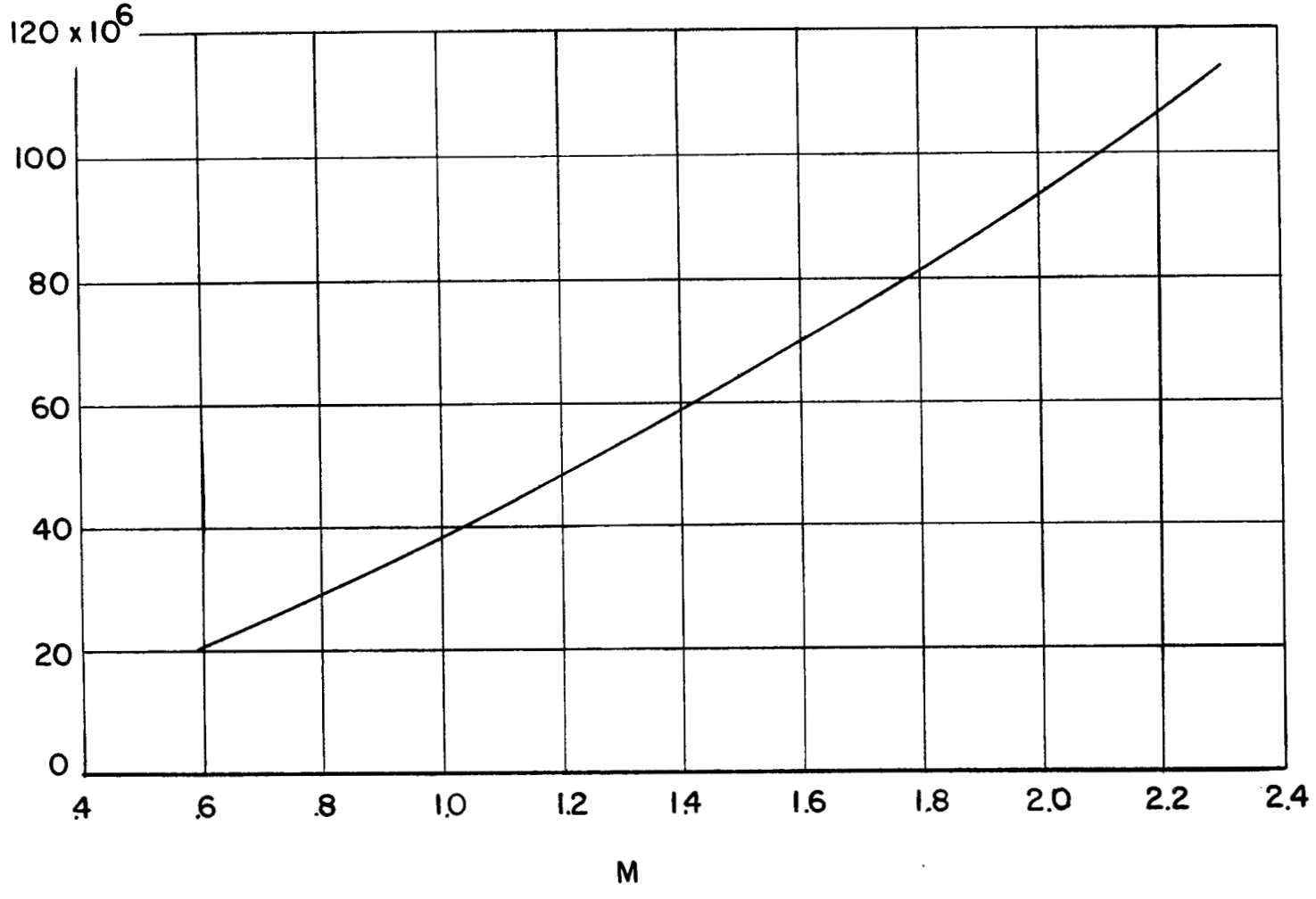

Figure 6.- Variation of Reynolds number, based on body length, with Mach number.

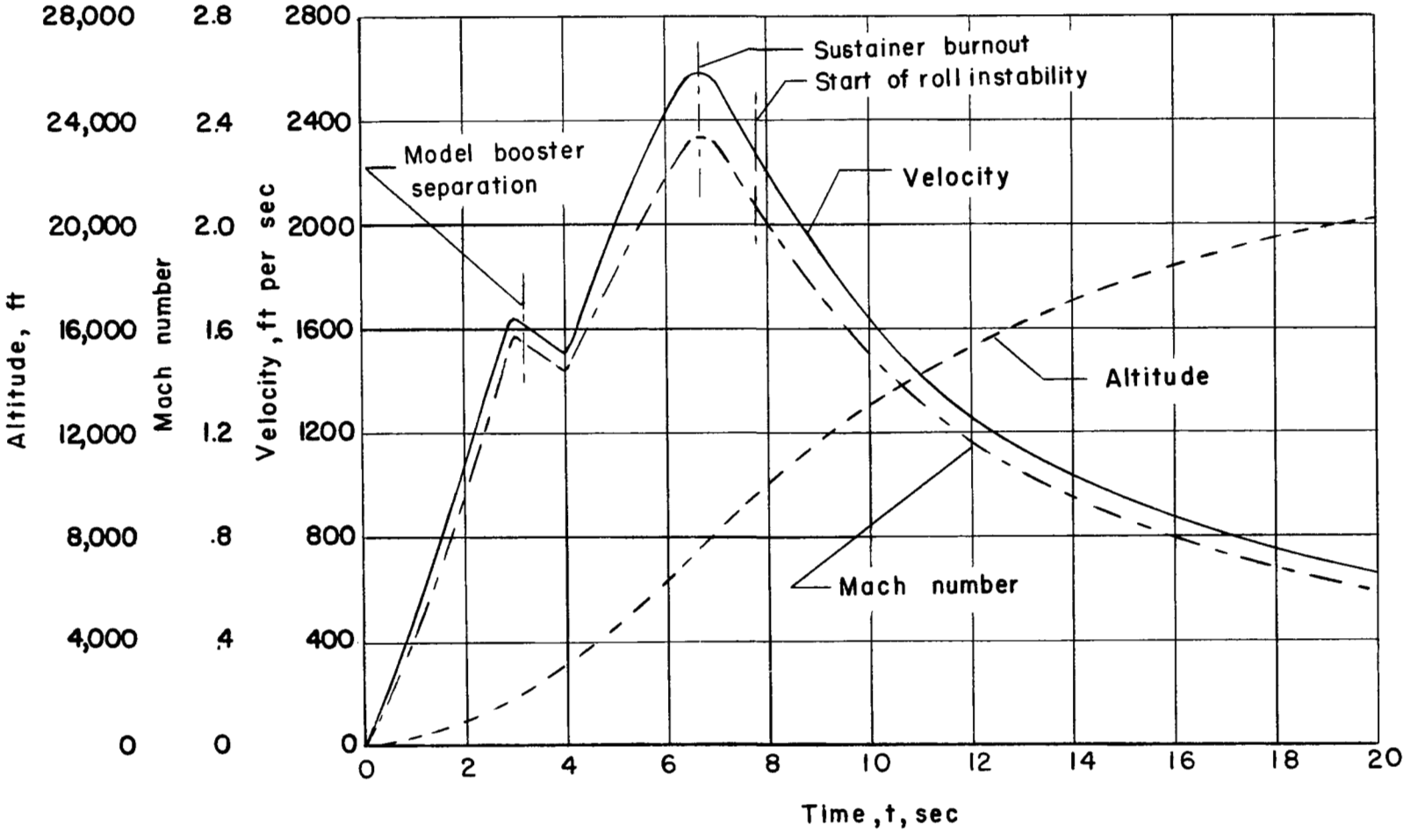

Figure 7.- Variation of velocity, Mach number, and altitude with time for model tested.

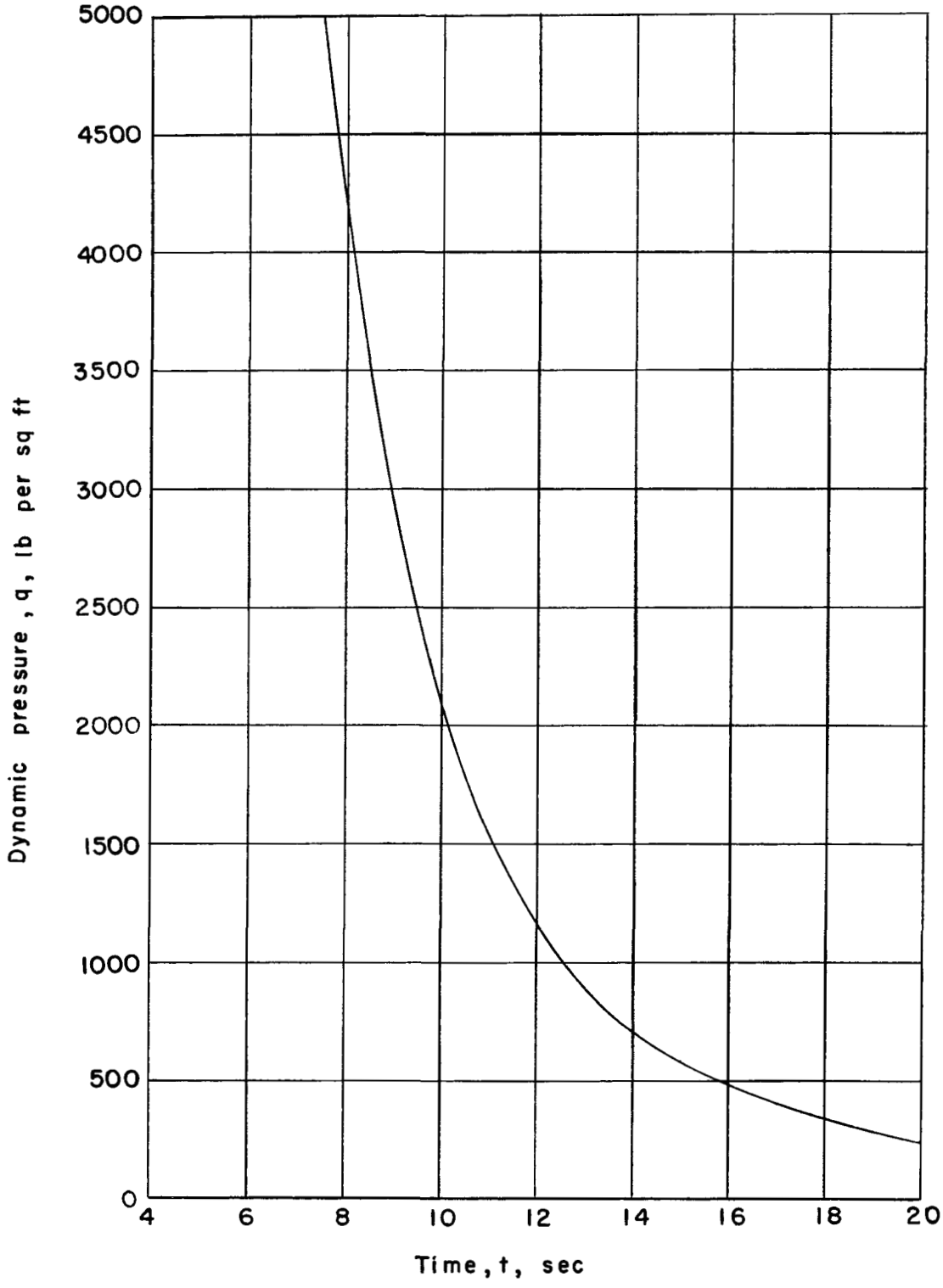

Figure 8.- Variation of dynamic pressure with time for model tested.

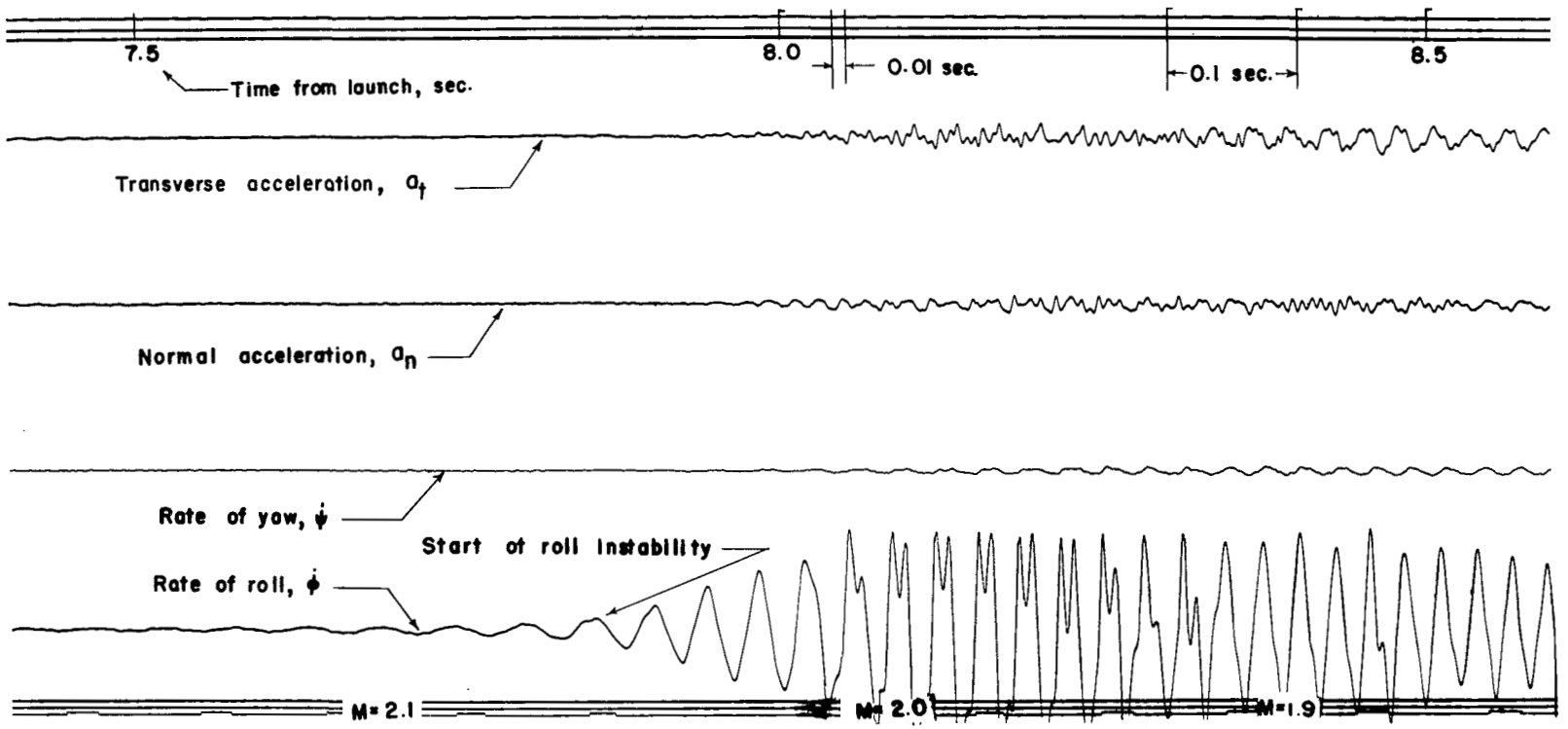

(a) Time, 7.5 to 8.5 sec.

Figure 9.- Portions of telemeter record obtained from model tested.

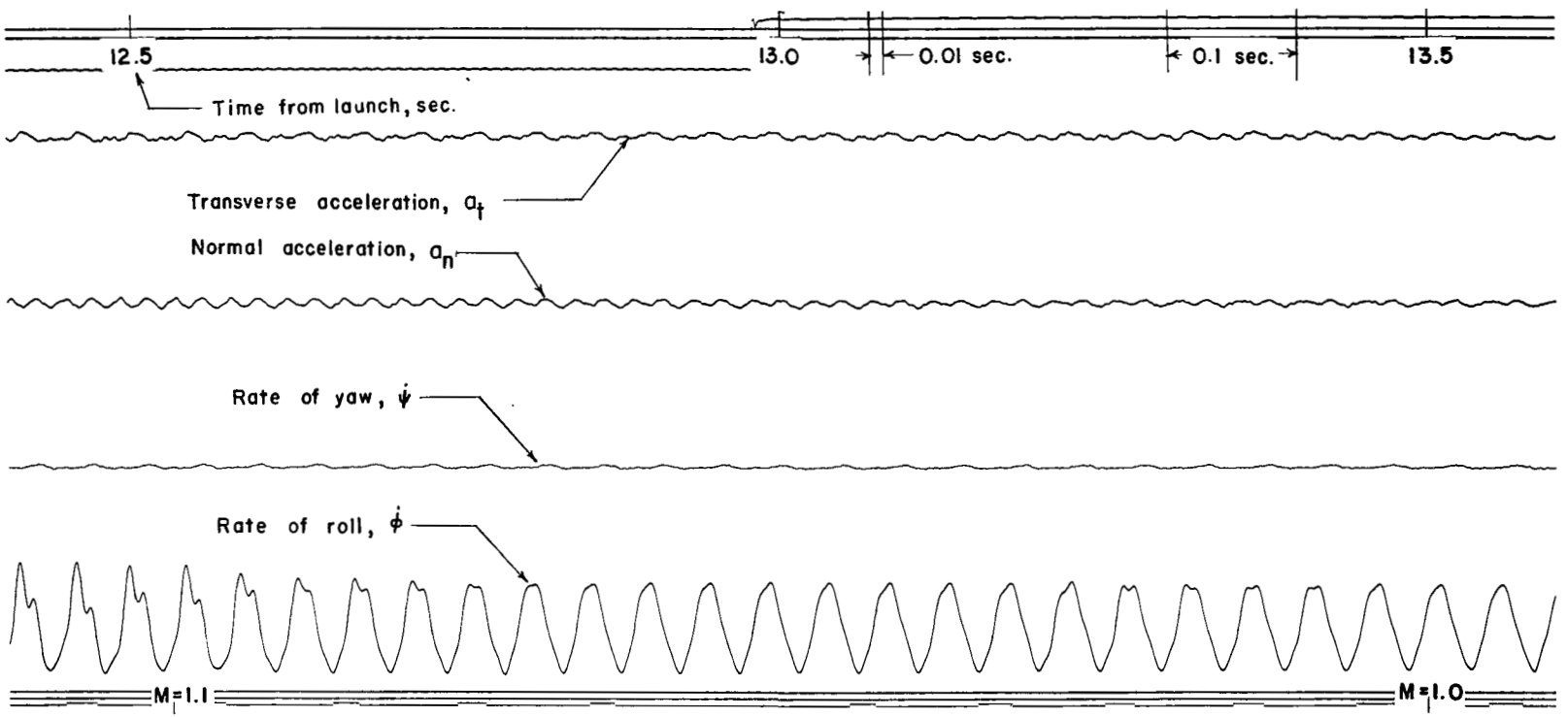

(b) Time, 12.5 to 13.5 sec.

Figure 9.- Continued.

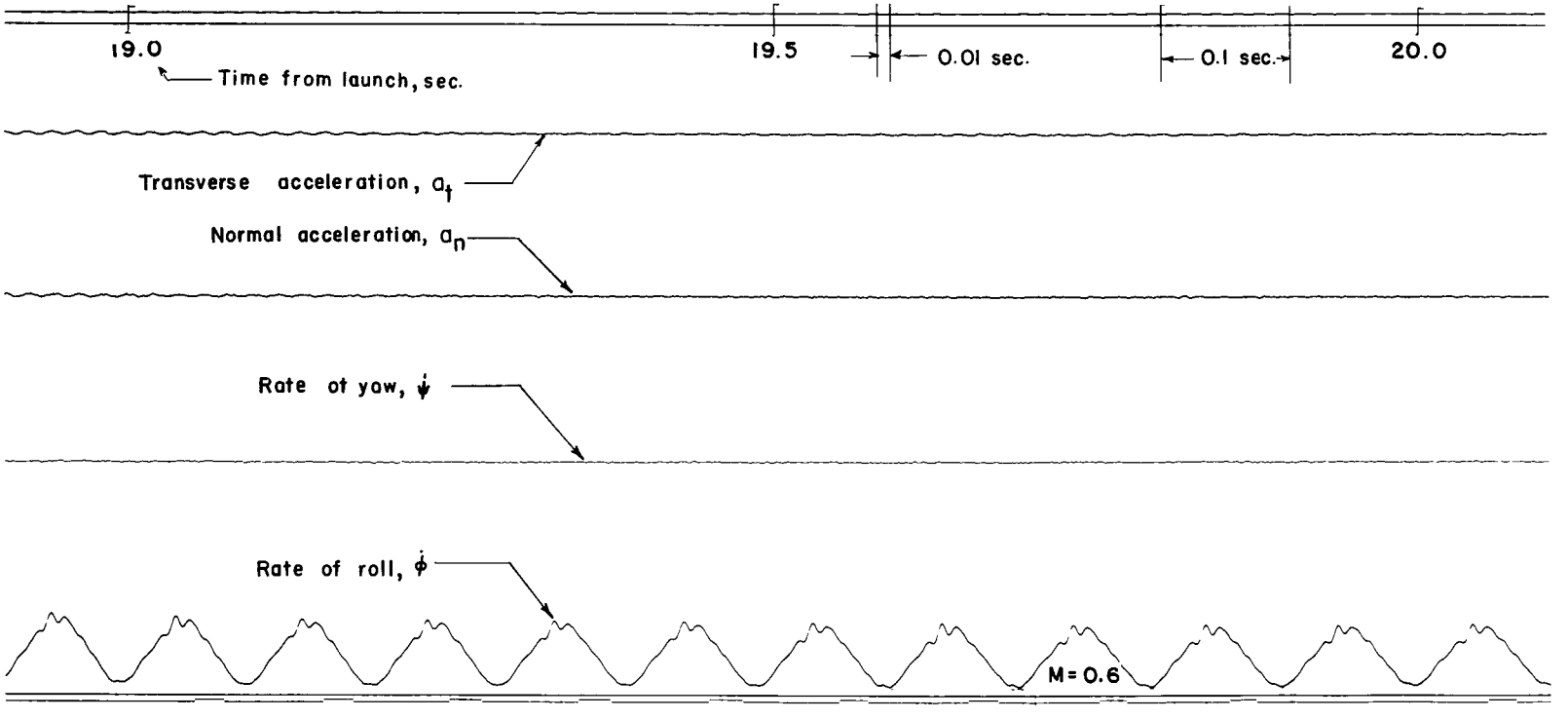

(c) Time, 19.0 to 20.0 sec.

Figure 9.- Concluded.

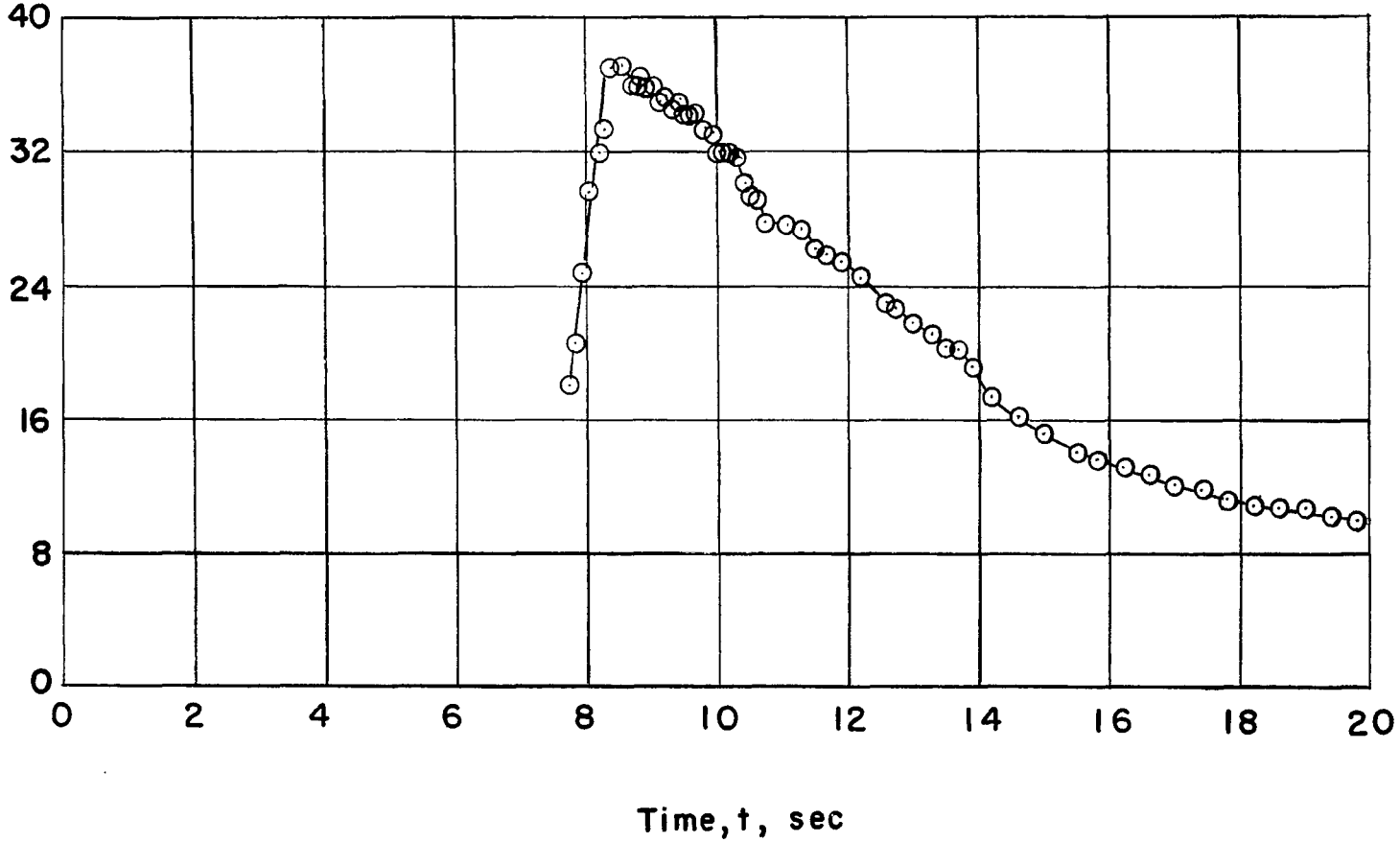

Figure 10.- Variation of the roll-velocity frequency with time for model tested.

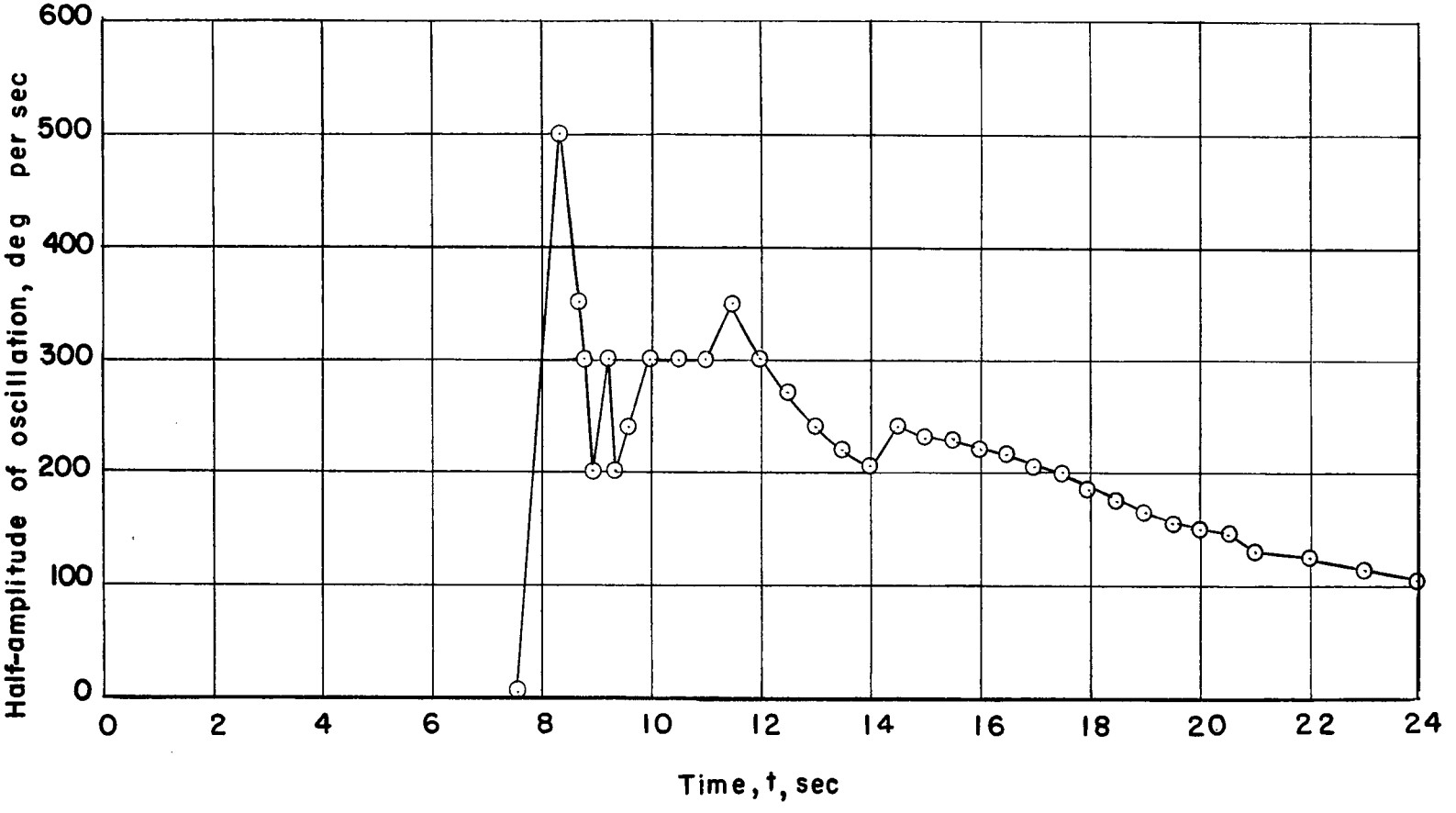

Figure 11.- Variation of the half-amplitude of the roll-velocity envelope with time for model tested.

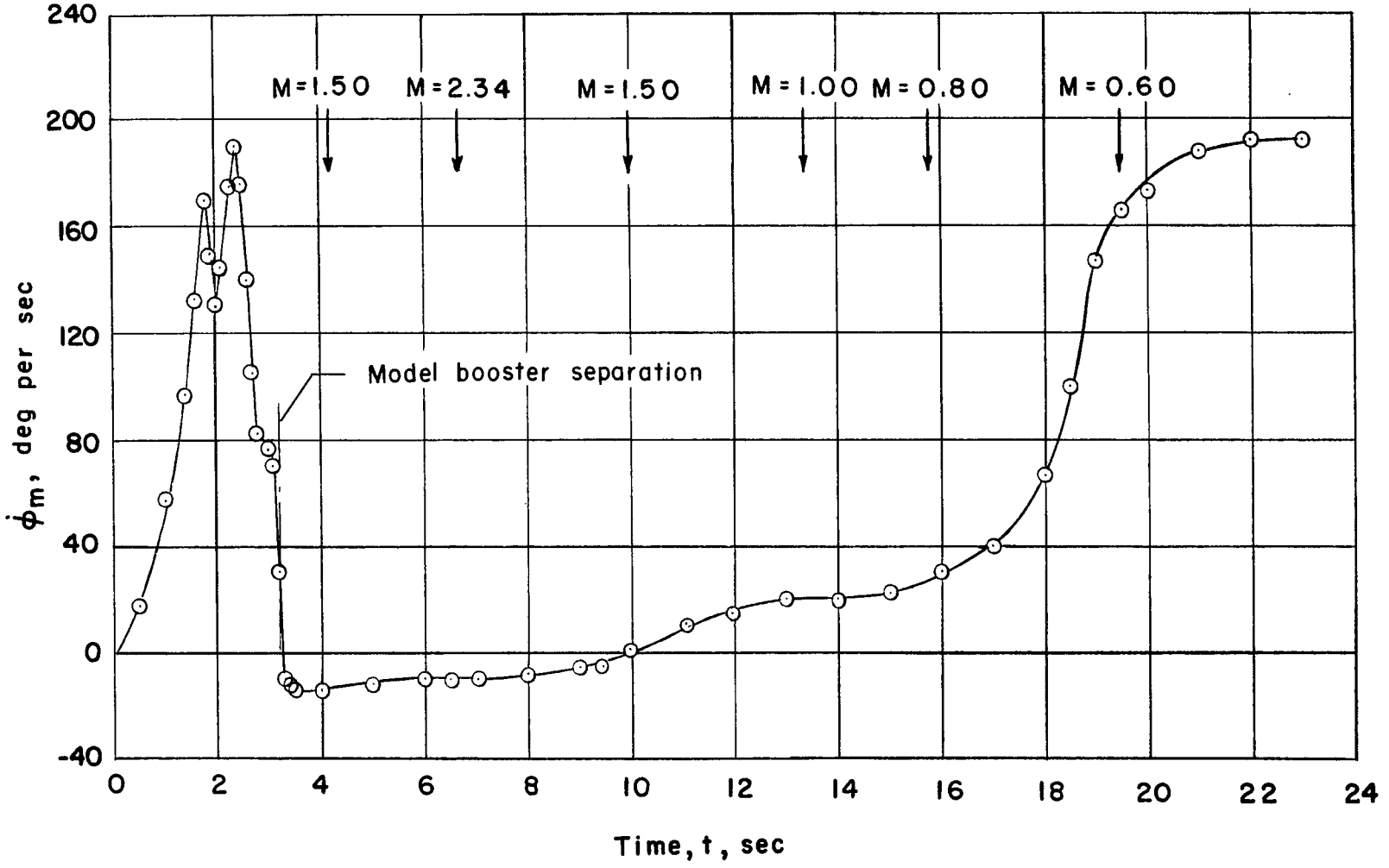

Figure 12.- Variation of the mean value of the roll-velocity envelope with time for model tested.

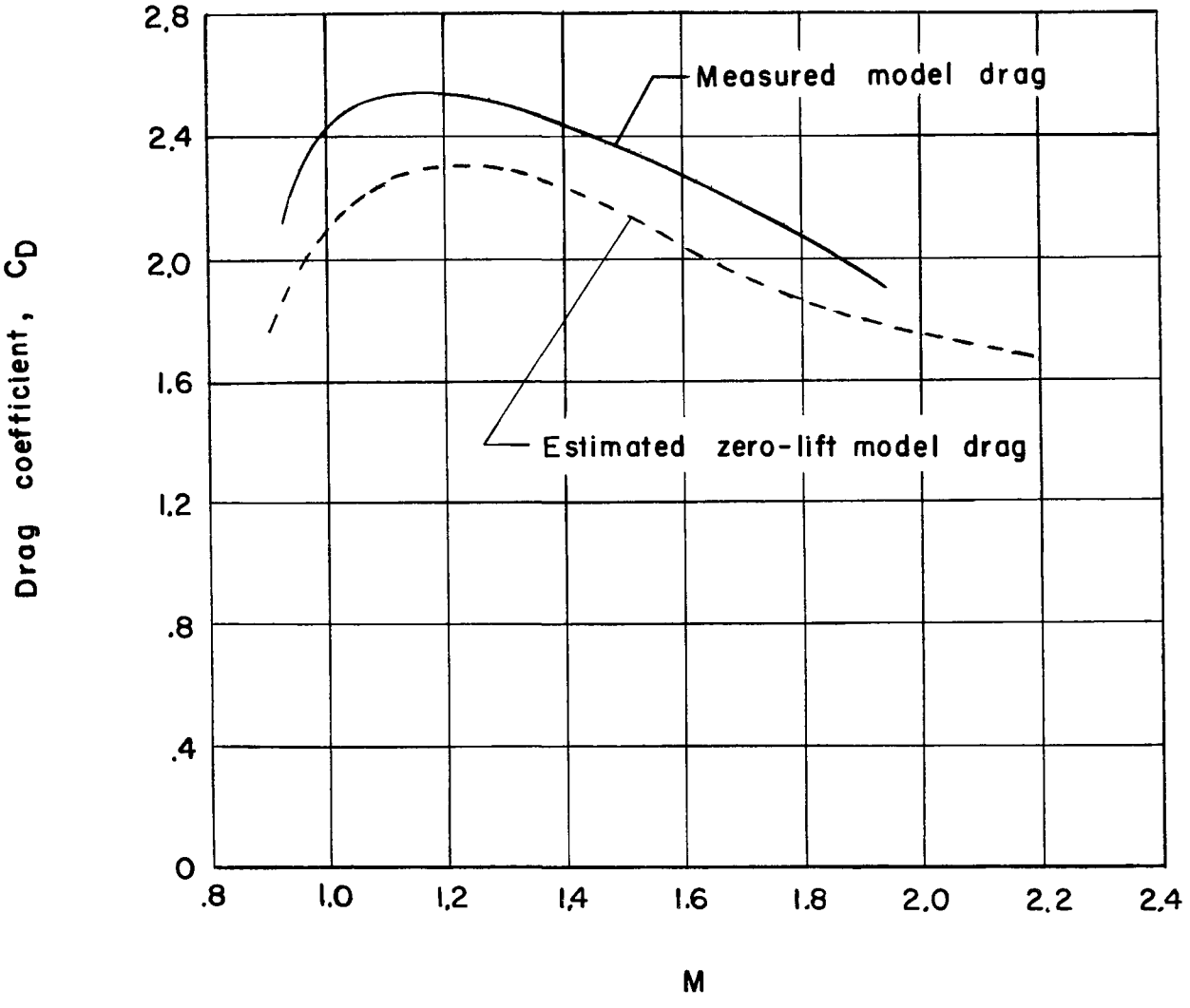

Figure 13.- Variation of the drag coefficient with Mach number for model tested.

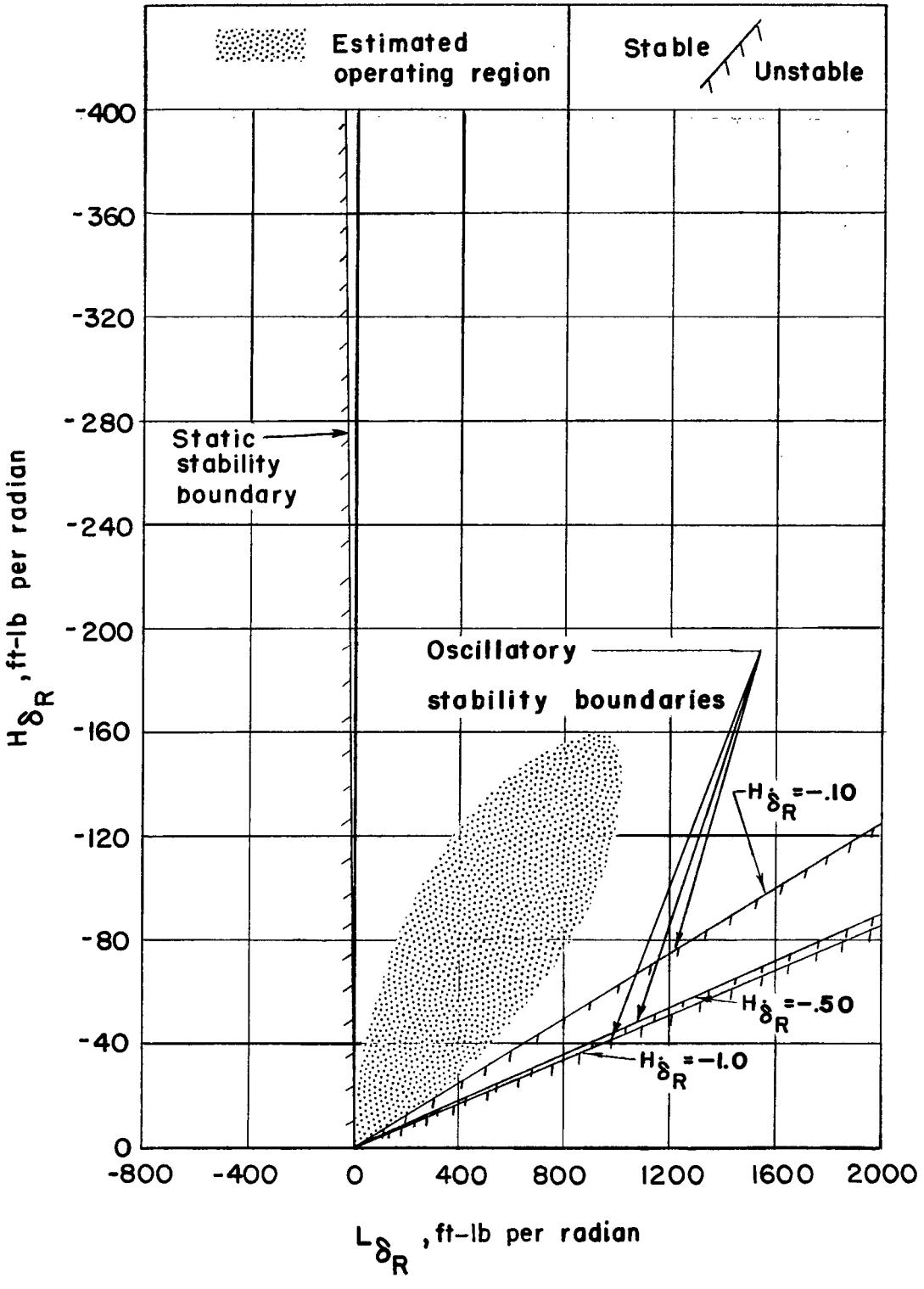

Figure 14.- Stability-boundary plots showing the effect of control surface damping. Gyro-wheel spin rate, 10,000 rpm; $L_{\dot{\phi}}$ = -0.05 ft-lb/radian/sec.

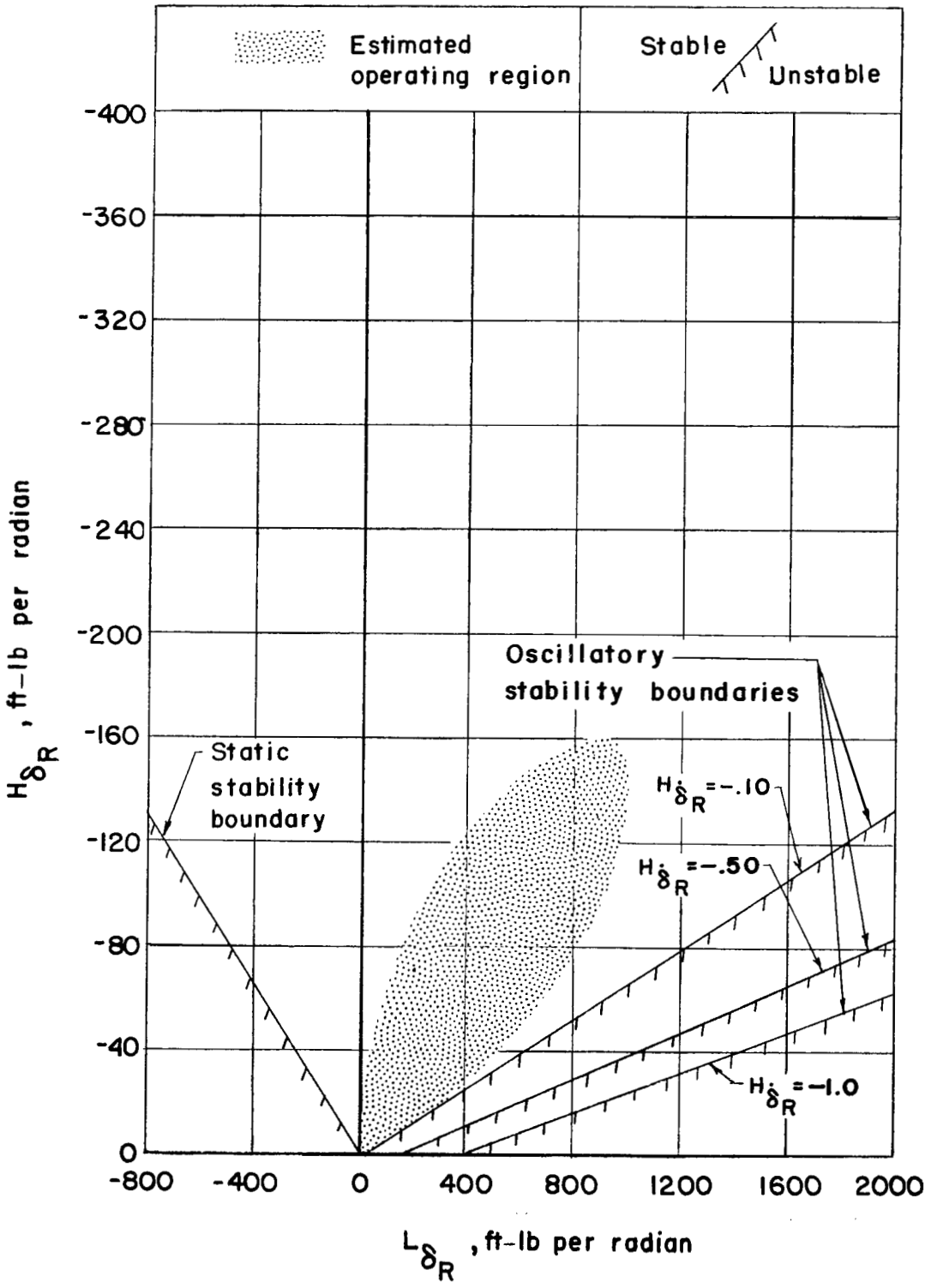

Figure 15.- Stability-boundary plots showing the effect of control surface damping. Gyro-wheel spin rate, 10,000 rpm; $L_{\dot{\phi}}$ = -5.0 ft-lb/radian/sec.

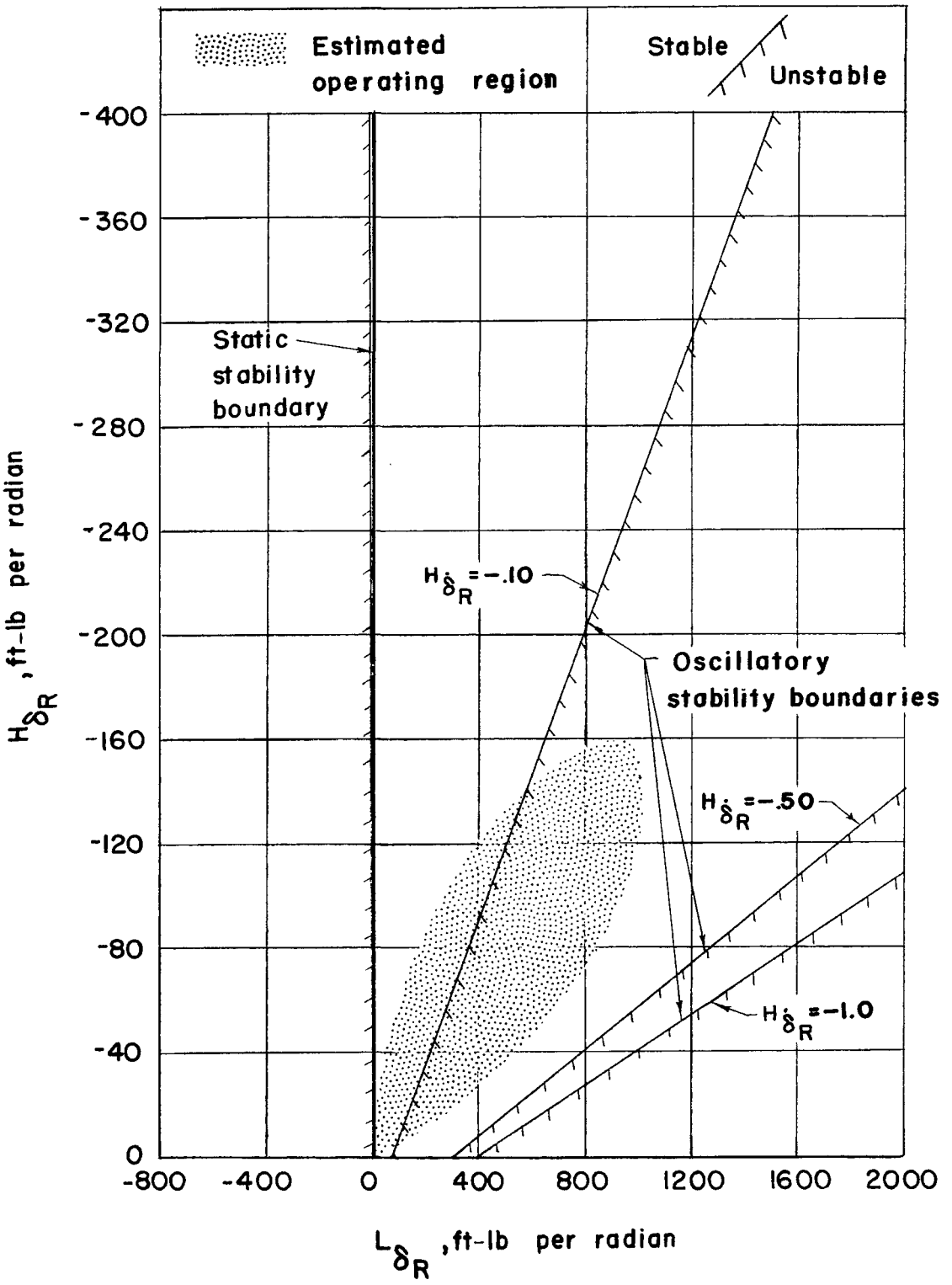

Figure 16.- Stability-boundary plots showing the effect of control surface damping. Gyro-wheel spin rate, 60,000 rpm; $L_{\dot{\varphi}}$ = -0.05 ft-lb/radian/sec.

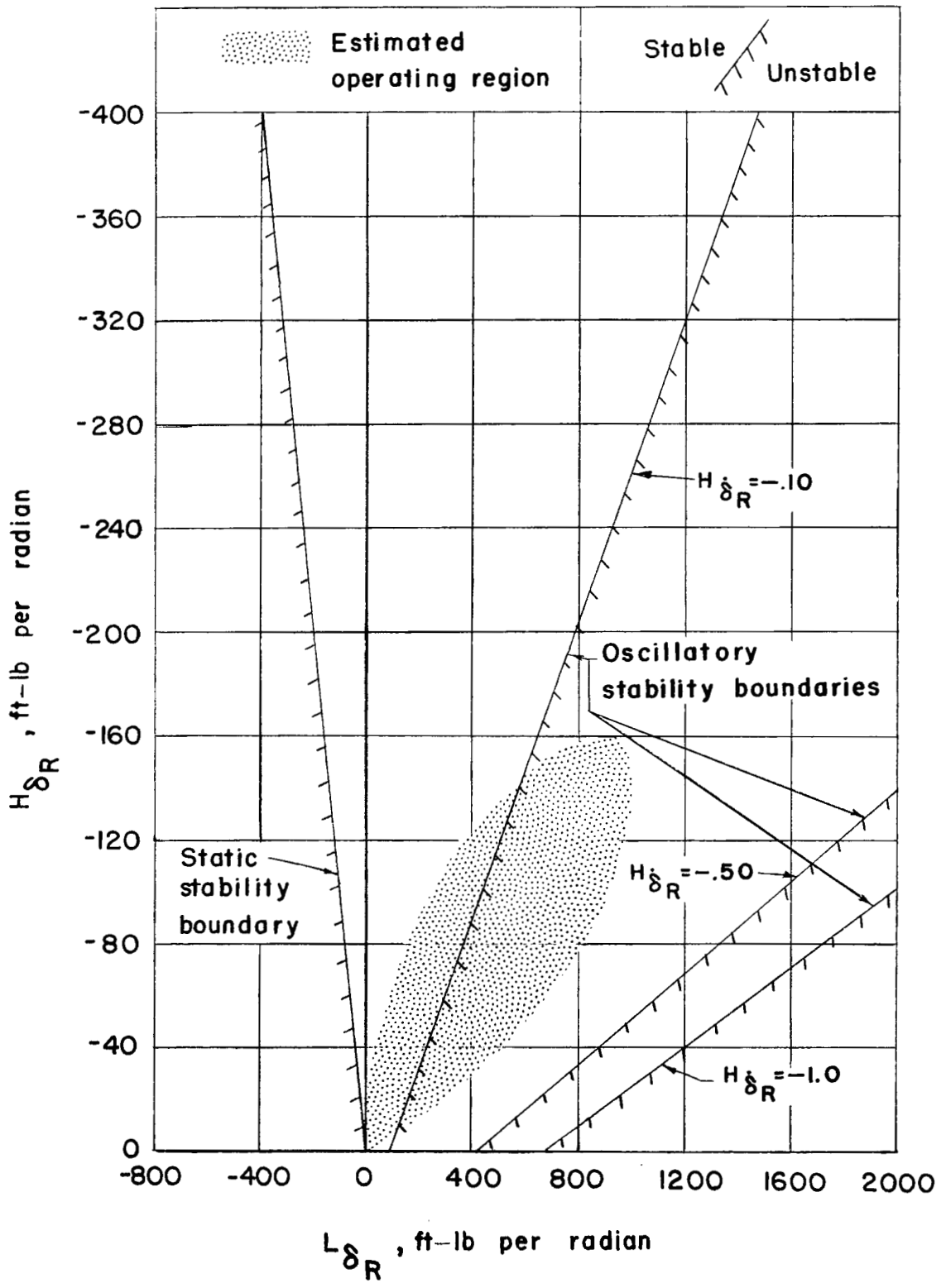

Figure 17.- Stability-boundary plots showing the effect of control surface damping. Gyro-wheel spin rate, 60,000 rpm; $L_{\dot{\phi}}$ = -5.0 ft-lb/radian/sec.

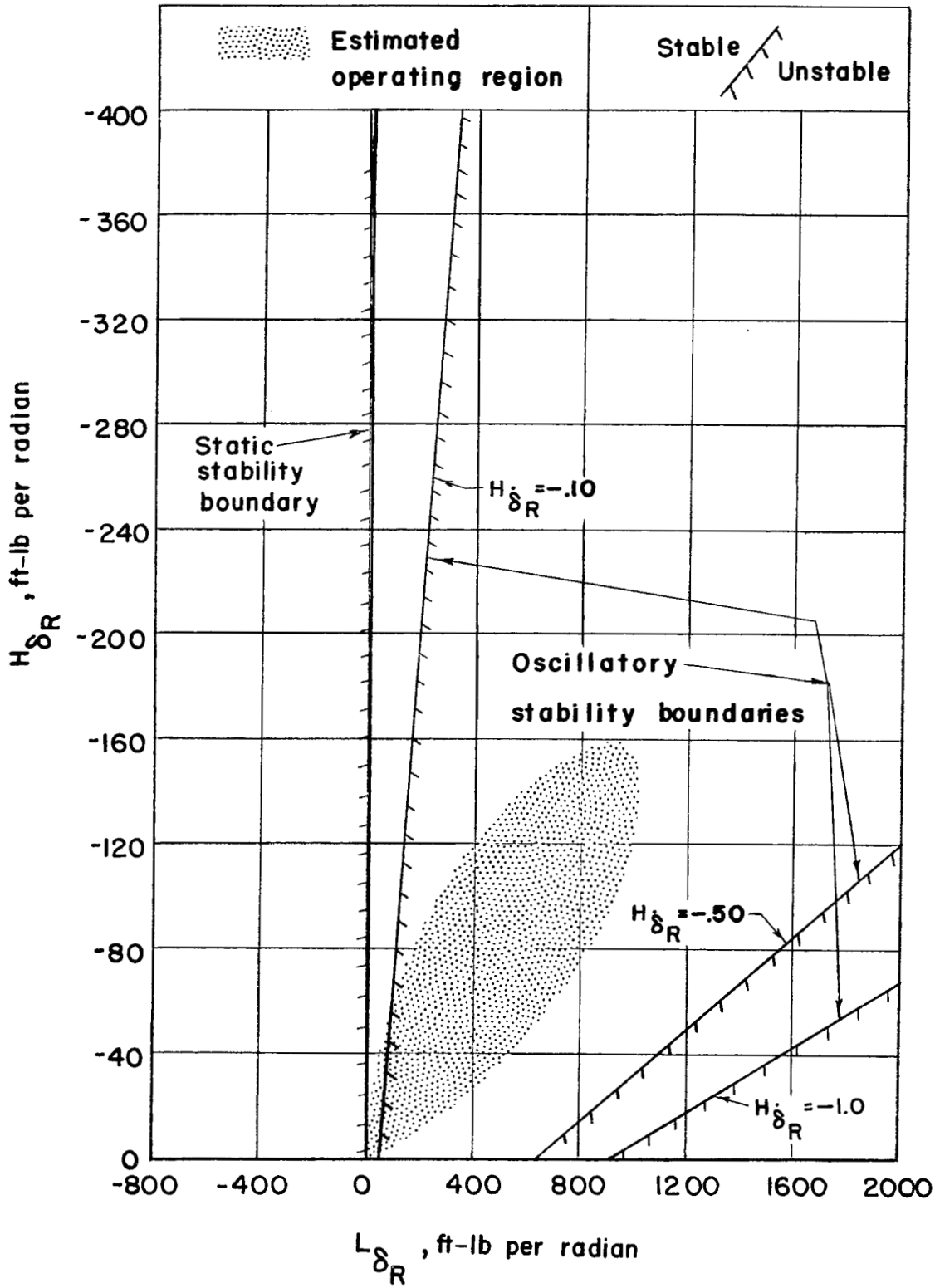

Figure 18.- Stability-boundary plots showing the effect of control surface damping. Gyro-wheel spin rate, 100,000 rpm; $L_{\dot{\phi}}$ = -0.05 ft-lb/radian/sec.

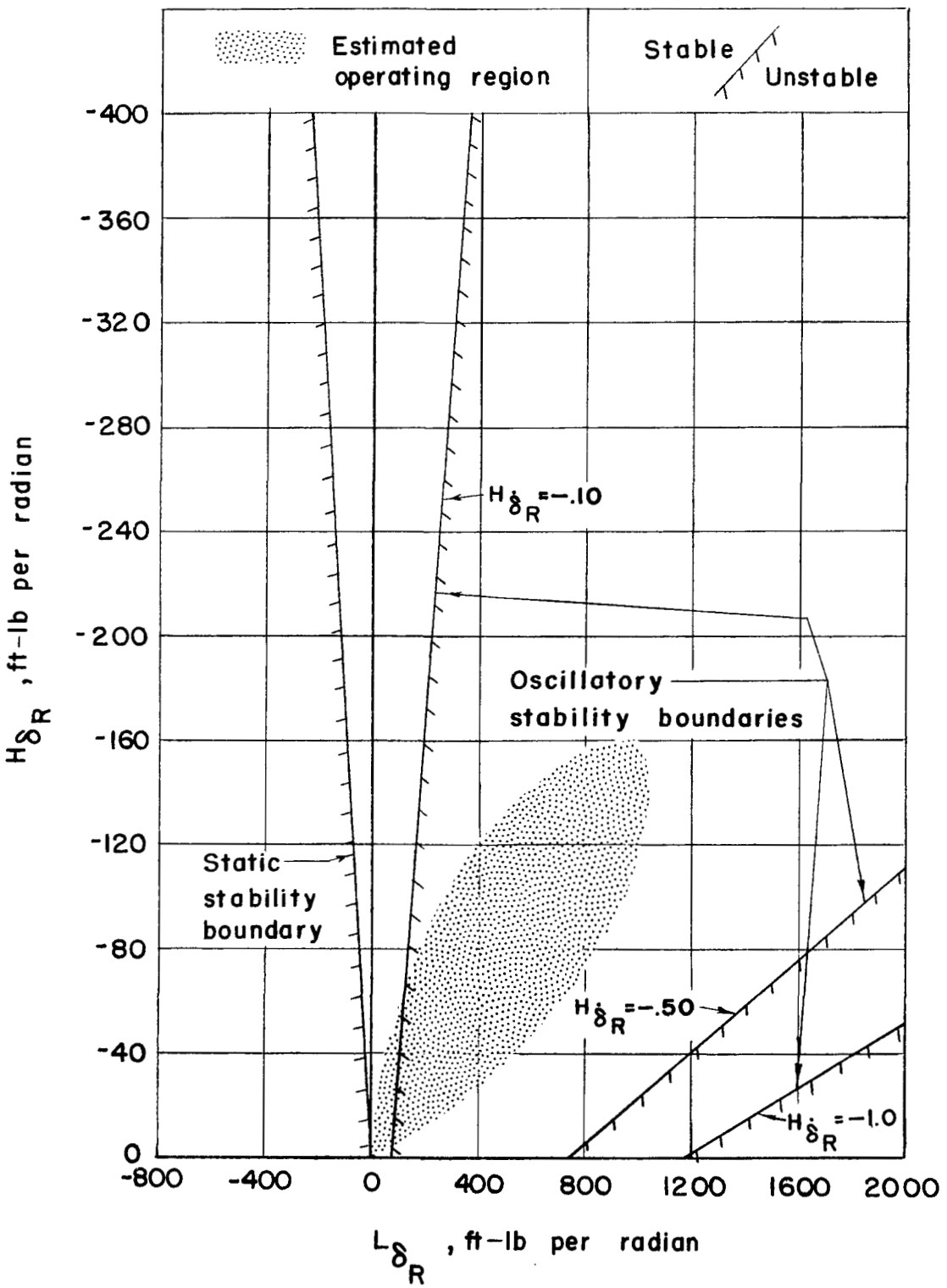

Figure 19.- Stability-boundary plots showing the effect of control surface damping. Gyro-wheel spin rate, 100,000 rpm; $L_{\dot{\phi}}$ = -5.0 ft-lb/radian/sec.

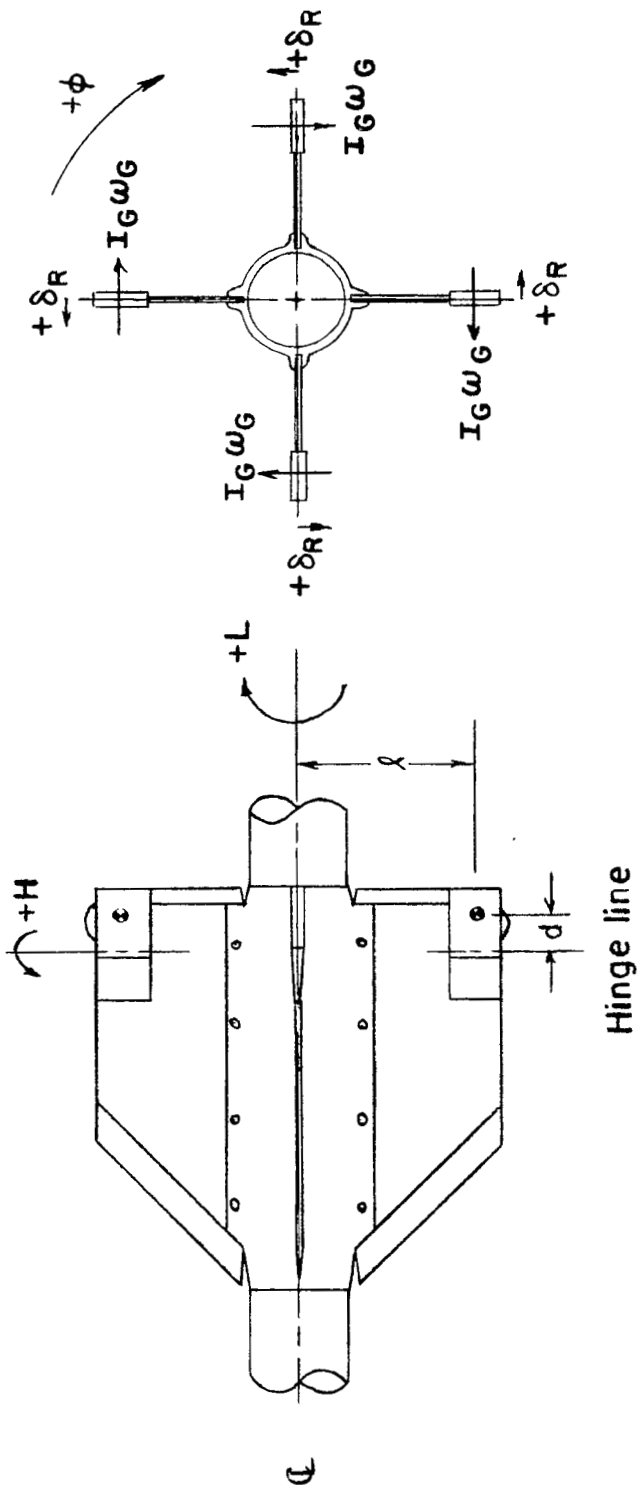

Figure 20.- Sketch of the SIDEWINDER missile showing rollerons and the assumed positive directions of moments and angles.